The Astrophysical Journal, 835:126 (5pp), 2017 February 1 doi:10.3847/1538-4357/835/2/126


# H I-to-$H_2$ Transition Layers in the Star-forming Region W43

Shmuel Bialy[1], Simon Bihr[2], Henrik Beuther[2], Thomas Henning[2], and Amiel Sternberg[1]
[1] Raymond and Beverly Sackler School of Physics & Astronomy, Tel Aviv University, Ramat Aviv 69978, Israel; shmuelbi@mail.tau.ac.il
[2] Max Planck Institute for Astronomy, Königstuhl 17, D-69117 Heidelberg, Germany
*Received 2016 November 7; revised 2016 December 6; accepted 2016 December 7; published 2017 January 23*

## Abstract

The process of atomic-to-molecular (H I-to-$H_2$) gas conversion is fundamental for molecular-cloud formation and star formation. 21 cm observations of the star-forming region W43 revealed extremely high H I column densities, of 120–180 $M_\odot$ pc$^{-2}$, a factor of 10–20 larger than predicted by H I-to-$H_2$ transition theories. We analyze the observed H I with a theoretical model of the H I-to-$H_2$ transition, and show that the discrepancy between theory and observation cannot be explained by the intense radiation in W43, nor be explained by variations of the assumed volume density or $H_2$ formation rate coefficient. We show that the large observed H I columns are naturally explained by several (9–22) H I-to-$H_2$ transition layers, superimposed along the sightlines of W43. We discuss other possible interpretations such as a non-steady-state scenario and inefficient dust absorption. The case of W43 suggests that H I thresholds reported in extragalactic observations are probably not associated with a single H I-to-$H_2$ transition, but are rather a result of several transition layers (clouds) along the sightlines, beam-diluted with diffuse intercloud gas.

*Key words:* galaxies: star formation – ISM: clouds – ISM: individual objects (W43) – ISM: structure – photon-dominated region (PDR)

## 1. Introduction

The transition of interstellar gas from atomic form (H I) to molecular ($H_2$) is of fundamental importance for the process of star formation, and has been studied via analytic modeling (e.g., Federman et al. 1979; Sternberg & Dalgarno 1989; Goldsmith et al. 2007; Krumholz et al. 2008; McKee & Krumholz 2010; Sternberg et al. 2014; Liszt 2015; Bialy & Sternberg 2016), hydrodynamical simulations (e.g., Robertson & Kravtsov 2008; Gnedin et al. 2009; Lagos et al. 2015; Valdivia et al. 2016), and observations (e.g., Savage et al. 1977; Reach et al. 1994; Gillmon et al. 2006; Lee et al. 2012; Noterdaeme et al. 2016).

Motte et al. (2014, hereafter M14) and Bihr et al. (2015, hereafter B15) studied the H I and $H_2$ gas in the W43 star-forming complex. W43 ($l = 29.^\circ2$–$31.^\circ5$, $|b| \leqslant 1^\circ$) is a region of very active star formation, containing many molecular clouds as well as atomic gas, with a total mass of atomic plus molecular gas of $\sim 10^7\ M_\odot$ (Motte et al. 2003; Ngûyen Luong et al. 2011; Carlhoff et al. 2013; B15). Based on parallax measurements of water and methanol masers, the distance to W43 is $d = 5.5 \pm 0.5$ kpc (Zhang et al. 2014), placing it at the intersection of the Galactic bar with the first spiral arm (Ngûyen Luong et al. 2011).

B15 reported on extremely large H I column densities, $\Sigma_{\rm H\,I,obs}$ 120–180 $M_\odot$ pc$^{-2}$, in W43. As shown by M14 and B15, the observed H I columns strongly exceed the columns theoretically expected from single-cloud H I-to-$H_2$ transition models. In such models (e.g., Krumholz et al. 2009, hereafter K09; McKee & Krumholz 2010; Sternberg et al. 2014, hereafter S14), the H I-to-$H_2$ transitions are computed assuming a balance between far-UV photodissociation and molecular formation, and accounting for the rapid attenuation of the radiation field due to $H_2$ self-shielding and dust absorption. For solar metallicity, the maximal predicted H I columns are $\sim 10\ M_\odot$ pc$^{-2}$, far less than observed in W43.

In this paper we analyze the H I columns in W43. We employ the S14 analytic model for the equilibrium H I columns produced in the transition layers, as functions of the field intensity, gas density, grain properties, and metallicity. The S14 and K09 models are very similar in their predictions for the H I columns (see Section 4 in S14 for a comparison of the planar versus spherical geometry). We show that the simplest and most likely explanation for the large observed H I columns is that several H I-to-$H_2$ transition layers are superimposed along the sightlines. This possible interpretation was already noted by M14.

The structure of the paper is as follows. We present the observations in Section 2. In Section 3 we analyze the data and estimate the number of H I-to-$H_2$ transition layers. We discuss the implications of our analysis and alternative scenarios in Section 4. We conclude in Section 5.

## 2. Observations

The analyzed H I data are based on observations of "the H I, OH, Recombination line survey of the Milky Way" (THOR; B15; Beuther et al. 2016). For the H I column density of W43, it is crucial to correct for 21 cm optical depth, as well as for weak diffuse continuum emission, otherwise the measured H I mass is underestimated by at least a factor of 2.4 (B15). The measured (corrected) H I column density map is shown in the left panel of Figure 1. The H I column density typically ranges between 120 and 180 $M_\odot$ pc$^{-2}$. We note that the corrected H I column density does not decrease toward the center as reported by previous studies (Ngûyen Luong et al. 2011), assuming optically thin H I emission. The molecular gas, as inferred from dust observations, is shown in the right panel of Figure 1 (Nguyen-Luong et al. 2013). It is much clumpier than the H I, and may be decomposed into ∼20 subclouds (Carlhoff et al. 2013). The $H_2$ column densities typically range within ~100–500 $M_\odot$ pc$^{-2}$ with peak values

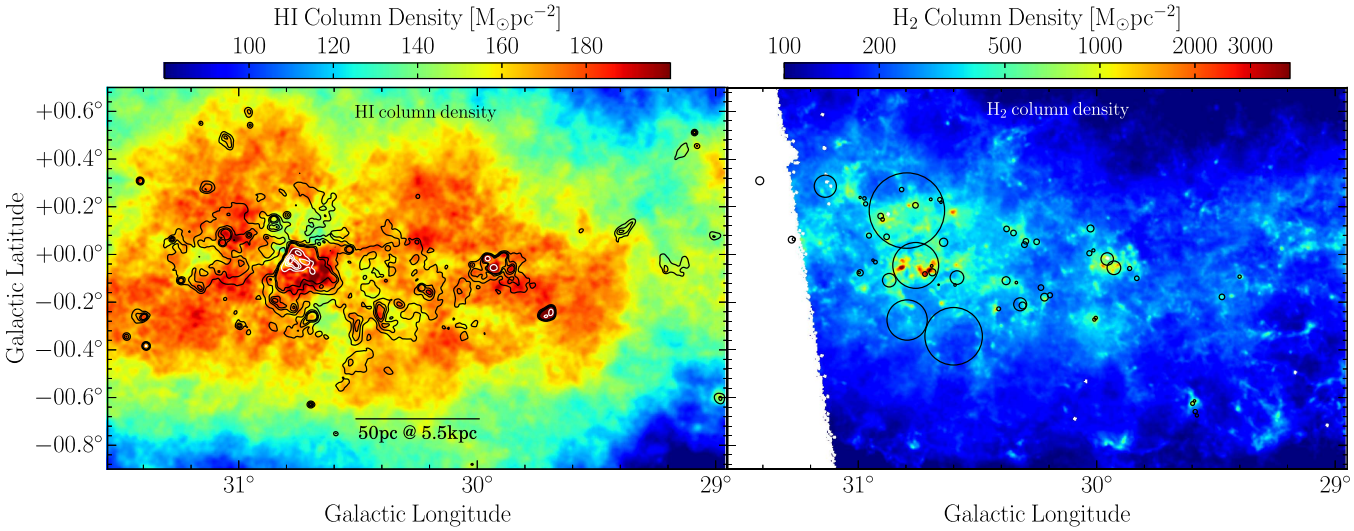


**Figure 1.** Left panel: H I column density taken from Bihr et al. (2015), corrected for optical depth effects and the continuum emission. The contours indicate the 1.4 GHz continuum emission (black contours: 10, 30, and 70 K; white contours: 200, 400, 600, and 800 K). Right panel: $H_2$ column density, based on *Herschel* dust observations from Nguyen-Luong et al. (2013). The black circles indicate H II regions taken from Anderson et al. (2014).

reaching $\sim$3000 $M_\odot$ pc$^{-2}$ at the cores (Carlhoff et al. 2013; Nguyen-Luong et al. 2013; B15).

To appreciate the high level of star formation activity in the region, the white circles in the right panel of Figure 1 indicate H II regions, taken from the catalog of Anderson et al. (2014), having distance estimates consistent with W43 ($d \approx 4$–8 kpc). The contours in the left panel indicate the 1.4 GHz continuum emission. The relatively high dust temperatures $T_{\rm dust} \approx 23$–27 K (higher than typical $T_{\rm dust} \lesssim 20$ K; Reach et al. 1995; Draine 2011) reported by Nguyen-Luong et al. (2013) also suggest intense far-UV irradiation (see Section 3.1).

## 3. Analysis

We analyze the observed H I column densities in W43 using the S14 steady-state H I-to-$H_2$ transition model. The S14 model assumes optically thick slabs of uniform density, irradiated by beamed or unidirectional far-UV flux. For a two-sided slab and isotropic irradiation, the H I column density is

$$\Sigma_{\rm H\,I} = \frac{6.71}{\tilde{\sigma}_g} \ln\left(\frac{\alpha G}{3.2} + 1\right) M_\odot \ {\rm pc}^{-2}, \quad (1)$$

where $\tilde{\sigma}_g \equiv \sigma_g/(1.9 \times 10^{-21}\ {\rm cm}^2)$ is the dust absorption cross section per hydrogen nucleus in the Lyman–Werner (LW) dissociation band (11.2–13.6 eV), normalized to a fiducial Galactic value (i.e., typically $\tilde{\sigma}_g \approx 1$), $\alpha$ is the ratio of the unshielded $H_2$ dissociation rate to $H_2$ formation rate, and $G$ is an average $H_2$ self-shielding factor in dusty clouds (see S14, and Bialy & Sternberg 2016 for a thorough discussion). For a shape of the interstellar radiation spectrum like that of Draine (1978), and $H_2$ formation on dust grains,

$$\alpha G = 2.0\, I_{\rm UV} \left(\frac{30\ {\rm cm}^{-3}}{n}\right)\left(\frac{9.9}{1 + 8.9\tilde{\sigma}_g}\right)^{0.37}. \quad (2)$$

Here $n$ is the volume density and $I_{\rm UV}$ is the interstellar radiation intensity relative to the field of Draine (1978). For typical cold neutral medium (CNM) conditions, $\alpha G \simeq 2.6$ and it is weakly dependent on $\tilde{\sigma}_g$ (Bialy & Sternberg 2016). Importantly, Equation (1) is for a *single* two-sided slab (an H I–$H_2$–H I "sandwich," hereafter referred to as an "H I-to-$H_2$ transition layer").

Given the large extent of W43 ($\sim$100 $\times$ 200 pc), the wealth of molecular structures, and the many embedded radiation sources (Figure 1; Carlhoff et al. 2013), we argue that the observed H I gas is probably not attributed to a single H I-to-$H_2$ transition layer but is composed of several transition layers, superimposed along the W43 sightlines. The idea of several transition layers is further supported by the H I spectrum, which shows several distinct peaks (see Figure 10 in B15), and also by observations of [C II] 158 $\mu$m emission (Shibai et al. 1991, as further discussed in Section 4). The H I spectrum saturates at an optical depth of $\sim$3, and deeper observations of W43 are expected to reveal more structures. In Section 4 we also discuss alternative scenarios for the large observed H I columns in W43.

Assuming $\mathcal{N}$ transition layers along a sightline, the observed H I column density is given by

$$\Sigma_{\rm H\,I,obs} = \phi\, \mathcal{N}\, \Sigma_{\rm H\,I}, \quad (3)$$

where $\phi$ is a geometrical factor of order unity, and $\Sigma_{\rm H\,I}$ is the column density of a single H I-to-$H_2$ transition layer as given by Equation (1). Assuming that the H I-to-$H_2$ transition layers are slabs that are randomly oriented, $\phi = 1$. This is because a slab that is tilted by an angle $\theta$ relative to the plane of the sky will have a column density $\propto 1/\cos(\theta)$, but will also have an area filling factor $\propto \cos(\theta)$.

In Figure 2 we plot $\Sigma_{\rm H\,I}$ as a function of $\alpha G$ as given by Equation (1). Overplotted are the observed $\Sigma_{\rm H\,I,obs} \approx 120$–180 $M_\odot$ pc$^{-2}$(horizontal strip). The vertical strip is the realistic $\alpha G$ range estimated for W43 (see Section 3.1). Figure 2 (and Equation (1)) shows that for a single-cloud model to fit the observations, unrealistically large values of $\alpha G$ are required. This remained an unresolved puzzle in B15. In the rest of this section we estimate $\alpha G$ and obtain the mean H I column for a single transition layer in W43. We then constrain the number of transition layers along the sightlines using the observed H I columns combined with Equation (3).

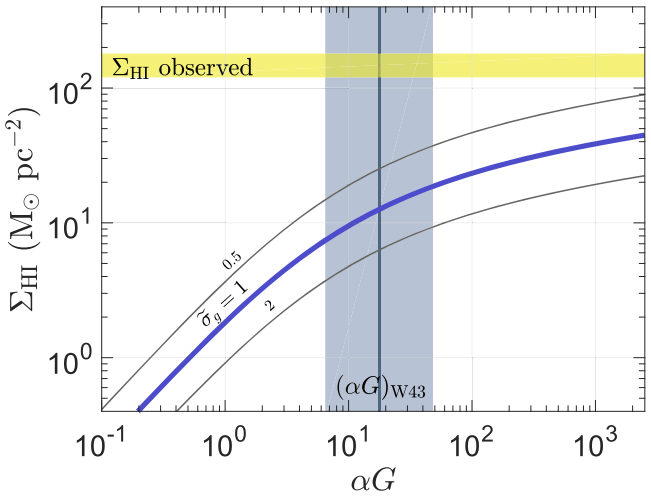


**Figure 2.** The H I column density of a single H I-to-$H_2$ transition layer as a function of the $\alpha G$ parameter, as given by Equation (1) assuming $\tilde{\sigma}_g = 1$ (thick blue curve) and factor-of-two variations about $\tilde{\sigma}_g = 1$ (thin gray). The vertical line and shaded strip are the median $\alpha G$ and the 68.3% range (i.e.,"1-sigma" error) for W43. The observed $\Sigma_{\rm H\,I,obs}$ in W43 (yellow shading) are larger by factors of ~10–20 than the theoretical curve.

### 3.1. αG *in W43*

To constrain $\alpha G$ in W43, we should approximate the UV intensity $I_{\rm UV}$ and the volume density $n$ for the H I gas of W43 (see Equation (2)). Adopting $T_{\rm dust} = 23$–$27$ K (Section 2) and assuming thermal equilibrium for the dust grains, $I_{\rm UV} = (T_{\rm dust}/T_0)^6$ with $T_0 = 17.5$ K (Draine 2011), we obtain $I_{\rm UV} = 5.2$–$13.5$. The modeling of the dust temperature is uncertain to within a factor of ~2, therefore we consider a wider range for $I_{\rm UV}$ and adopt $I_{\rm UV} = 3$–$30$.

We shall now obtain an approximation of the volume density $n$. Theoretically, the CNM ($n \approx 30$ cm$^{-3}$; Draine 2011) is expected to dominate the shielding and the H I-to-$H_2$ transition (K09, although see Bialy et al. 2015). For a CNM gas in thermal equilibrium with warm neutral medium (WNM), the volume density of the CNM is an increasing function of $I_{\rm UV}$ (Wolfire et al. 2003). For $I_{\rm UV} = 3$–$30$, Wolfire et al. (2003) suggest $n \sim 30$–$100$ cm$^{-3}$. From an observational point of view, by averaging the observed H I column densities over elliptical annuli and dividing by the equivalent radius, B15 estimated $n \approx 10$–$20$ cm$^{-3}$ for the H I gas in W43. This procedure assumes a gas of uniform density. For a clumpy medium the H I density values will increase. In summary, given the uncertainties, we adopt $n = 10$–$100$ cm$^{-3}$ for the atomic gas of W43.

We use Equation (2) and evaluate the $\alpha G$ probability distribution function (PDF) assuming that $\log n$ and $\log I_{\rm UV}$ are uniformly distributed within the adopted ranges, giving

$$(\alpha G)_{\rm W43} = 17.7^{+30.7}_{-11.2} \tag{4}$$

for the median $\alpha G$ and the "1-sigma" error (see the Appendix). The median and $1\sigma$ range are shown by the vertical line and shading in Figure 2. This $\alpha G$ was evaluated at $\tilde{\sigma}_g = 1$. Although the value of $\alpha G$ depends on the assumed $\tilde{\sigma}_g$, the dependence is weak, so for the case of simplicity we show the $\alpha G$ ranges only for $\tilde{\sigma}_g = 1$.

### 3.2. The Number of H I-to-$H_2$ Transition Layers

Adopting the $\alpha G$ range given by Equation (4), the column density of a single H I-to-$H_2$ transition layer is $\Sigma_{\rm H\,I} = 13^{+6}_{-5}/\tilde{\sigma}_g\ M_\odot$ pc$^{-2}$ (Equation (1)). Following Equation (3), the number of H I-to-$H_2$ transition layers is

$$\mathcal{N} = 13^{+9}_{-4}\left(\frac{\Sigma_{\rm H\,I,obs}}{160\ M_\odot\ {\rm pc}^{-2}}\right)\tilde{\sigma}_g \tag{5}$$

where $\Sigma_{\rm H\,I,obs}$ is an observed H I column. In Equation (5), the typical dust absorption cross section is $\tilde{\sigma}_g = 1$ (corresponding to $\sigma_g = 1.9 \times 10^{-21}$ cm$^2$). The value of $\tilde{\sigma}_g$ depends on the dust-to-gas ratio and the composition and size distribution of the dust grains. The metallicity and the dust-to-gas ratio typically increase with decreasing galactocentric distance, suggesting that $\tilde{\sigma}_g$ is possibly larger by up to a factor of ~2 in W43. The value of $\tilde{\sigma}_g$ depends also on the shape of the extinction curve. The fiducial value assumes $R_V \equiv A_V/E(B-V) = 3.1$ (appropriate for diffuse gas with $n \sim 100$ cm$^{-2}$); in dense regions ($n \gtrsim 10^3$ cm$^{-3}$) the dust-extinction curve becomes less steep toward the UV, and $\tilde{\sigma}_g$ may decrease by up to a factor of ≈2 (Draine 2003). Assuming an uncertainty range of $\tilde{\sigma}_g = 0.5$–$2$ and reevaluating the PDF of $\alpha G$, $\Sigma_{\rm H\,I}$, and $\mathcal{N}$, we obtain a larger median value and uncertainty range, $\mathcal{N} = 13^{+13}_{-6}(\Sigma_{\rm H\,I,obs}/160\ M_\odot\ {\rm pc}^{-2})$.

Based on this analysis, a typical fluctuation of the column density in the H I map may be approximated by $\Delta\Sigma_{\rm H\,I,obs}/\Sigma_{\rm H\,I,obs} \sim 1/\mathcal{N} \approx 5\%$–$12\%$, arising from sightlines that differ by a single transition layer. These values are in agreement with the observed H I map shown in Figure 1.

The length scale of W43 along the line of sight may be approximated through $\Delta z = \lambda_{\rm H\,I}\mathcal{N}$, where $\lambda_{\rm H\,I}$ is the characteristic H I scale given by

$$\lambda_{\rm H\,I} = 2\ \frac{1}{\sigma_g n} = 11.4\ \frac{1}{\tilde{\sigma}_g}\left(\frac{30\ {\rm cm}^{-3}}{n}\right){\rm pc}, \tag{6}$$

where the factor of two is for the two sides of the slab. For $\mathcal{N} = 9$–$21$ and $n = 30$ cm$^{-3}$, $\Delta z \sim 100$–$250$ pc, comparable to the projected dimensions of W43. This is only a lower limit on $\Delta z$ since the H I-to-$H_2$ transition layers may be spatially separated with diffuse atomic and ionized gas.

## 4. Discussion

We have shown that the observed H I column densities in W43 are naturally explained by a model of ~9–21 H I-to-$H_2$ transition layers superimposed along the W43 sightlines. Several transition layers are also expected from the clumpy molecular structure revealed by CO and dust, the high star formation activity, and the wealth of embedded radiation sources.

Several transition layers along the W43 sightlines were also inferred from [C II] 158 $\mu$m observations (Shibai et al. 1991). Assuming thermal balance between [C II] 158 $\mu$m cooling and photoelectric heating, Shibai et al. (1991) found $\mathcal{N} \sim 5$ (see their Section 4.4). However, they assumed a different geometry for the clouds (thin shells). To compare with our model, we modify their formula (their third equation in Section 4.4) to match our geometry of a

randomly oriented slab[3], giving

$$I_{[\mathrm{C\,II}]} \simeq 5.1 \times 10^{-6}\, \mathcal{N}\, I_{\mathrm{UV}}\ \mathrm{erg\ cm^{-2}\ s^{-1}\ sr^{-1}}. \quad (7)$$

Shibai et al. (1991) reported observations of $I_{[\mathrm{C\,II}]} = 7 \times 10^{-4}$ erg cm$^{-2}$ s$^{-1}$ sr$^{-1}$, implying $\mathcal{N} = 13.7(I_{\mathrm{UV}}/10)^{-1}$, consistent with our result $\mathcal{N} = 13^{+9}_{-4}$.

### 4.1. Model and Observational Limitations

The H I map of B15 was obtained by integrating the 21 cm observations over the "complete" velocity range of W43, $v_{\mathrm{lsr}} = 60$–$120$ km s$^{-1}$ (Ngûyen Luong et al. 2011). If part of the observed H I gas is unrelated to W43, or is very diffuse and extended, then $\Sigma_{\mathrm{H\,I,obs}}$ should be decreased, and the value of $\mathcal{N}$ will decrease accordingly. However, even if we consider only half of the observed $\Sigma_{\mathrm{H\,I}}$, still several H I-to-$H_2$ transitions are required.

In contrast to this, $\Sigma_{\mathrm{H\,I,obs}}$ could also be higher: B15 used the optical depth $\tau$ to correct $\Sigma_{\mathrm{H\,I,obs}}$. Because the absorption spectrum used saturates, the measured optical depth is a lower limit and hence $\Sigma_{\mathrm{H\,I,obs}}$ is a lower limit as well.

The S14 theory assumes chemical equilibrium. The longest timescale involved is the $H_2$ formation time, $\tau_{H_2} = 1/(2Rn)$, where $R$ is the $H_2$ formation rate coefficient. For $R = 3 \times 10^{-17}$ cm$^{-3}$ s$^{-1}$ and $n = 30$ cm$^{-3}$, $\tau_{H_2} = 18$ Myr. In a turbulent medium the $H_2$ formation time may be much shorter, ~1–2 Myr (Glover & Mac Low 2007).

The S14 model assumes a gas of uniform density for the H I shielding envelopes. In real astrophysical environments the gas is highly turbulent, producing large density fluctuations. However, S. Bialy et al. (2016, in preparation) find that even in highly turbulent supersonic gas, the median $\Sigma_{\mathrm{H\,I}}$ value remains very close to the homogeneous solution given by Equation (1). Moreover, for large $\alpha G$ the spread in $\Sigma_{\mathrm{H\,I}}$ is small (typically within a factor of ~2).

Equation (2) for $\alpha G$ assumes an $H_2$ formation rate coefficient of $R = 3 \times 10^{-17}$ cm$^3$ s$^{-1}$ and a spectral shape like that of Draine (1978). The value of $R$ is highly uncertain. However, the fact that the dependence of $\Sigma_{\mathrm{H\,I}}$ on $\alpha G$ is logarithmic (Equation (1)) makes our analysis robust to variations in all parameters entering $\alpha G$; the UV intensity, spectral shape, volume density, $H_2$ formation rate coefficient, and $H_2$ self-shielding function.

### 4.2. Alternative Explanations for the Large H I Columns

M14 and B15 analyzed the observed H I-to-$H_2$ column densities using the K09 equilibrium model and also found that the observed $\Sigma_{\mathrm{H\,I}}$ values are far in excess of those predicted theoretically. This is not surprising since like the S14 model, the K09 model is also a steady-state model that is applicable to a single cloud. The M14 and B15 studies proposed alternative explanations for the discrepancy between theory and observations.

B15 suggested that the intense UV radiation field in W43 may account for the large observed $\Sigma_{\mathrm{H\,I,obs}}$. Following Equation (1), we see that $\alpha G$ must be extremely large for a single H I-to-$H_2$ transition to reproduce the observed H I column densities. For example, for $\Sigma_{\mathrm{H\,I,obs}} = 120$–$180\ M_\odot$ pc$^{-2}$, and assuming $\tilde{\sigma}_g = 1$, $\alpha G$ is between $1.9 \times 10^8$ and $1.4 \times 10^{12}$ respectively, requiring unrealistically high ratios of $I_{\mathrm{UV}}$ to density (see Equation (2)).

A single equilibrium transition layer may be consistent with observations if the dust absorption cross section ($\tilde{\sigma}_g$) is significantly reduced. For the $1\sigma$ $\alpha G$ range, $\tilde{\sigma}_g = 0.05$–$0.11$ reproduces the observed $\Sigma_{\mathrm{H\,I}} = 160\ M_\odot$ pc$^{-2}$. Such low dust absorption cross sections may be a result of a reduced dust-to-gas ratio or an abnormal population of dust grains that is selectively inefficient in far-UV absorption. However, this is unlikely given the very large deviation from typical values in the interstellar medium. The effectiveness of dust absorption may also be reduced by dust–gas separation resulting from nonisotropic radiation (Weingartner & Draine 2001). However, the timescales involved are very long: $t = 100\ r_{\mathrm{pc}}$ Myr for 0.1 $\mu$m grains, where $r_{\mathrm{pc}}$ is the separation length in parsecs.

M14 identified three velocity gradients in the position–velocity map of W43, possibly indicative of inflowing gas streams. The large H I columns were then interpreted by M14 as dynamically accumulated atomic gas that has not yet had time to convert into $H_2$. In this scenario the accretion timescale must be short compared to the $H_2$ formation time, $\tau_{H_2} = 1$–$20$ Myr (Section 4.1), thus requiring a minimum inflow rate of $\dot{M}_{\mathrm{H\,I}} = 2.7$–$0.15\ M_\odot$ yr$^{-1}$ (assuming $M_{\mathrm{H\,I}} = 2.7 \times 10^6\ M_\odot$; B15). However, M14 were unable to estimate the gas inflow rates. Even if gas streams are present, they may be dense enough to already contain the equilibrium H I/$H_2$ interfaces and contribute to the total number $\mathcal{N} \approx 13$, estimated in Section 3.2.

The alternatives of photodissociated multiple layers versus a nonequilibrium atomic inflow may be distinguished by the presence or absence of infrared (IR) $H_2$ line emission. In the layers, far-UV radiation not only photodissociates $H_2$ but also populates excited $H_2$ rotational–vibrational levels, resulting in energetic cascade and IR emission. In contrast, for an atomic inflow there are no molecules to excite. Thus, our scenario predicts high IR line emissions, with an integrated flux being proportional to the observed H I column densities (Black & van Dishoeck 1987; Sternberg 1988). Such observations could confirm the predictions of our multislab model. To our knowledge, there are no current IR spectra of the $H_2$ ro-vibrational transitions in W43.

### 4.3. Comparison to Other H I Observations

A much less extreme example of enhanced H I columns may be found in the Perseus molecular cloud. Lee et al. (2015) reported $\Sigma_{\mathrm{H\,I,obs}} \approx 6$–$9\ M_\odot$ pc$^{-2}$, and Bialy et al. (2015) showed that these values are 2–3 times larger than what is theoretically expected for CNM conditions. Bialy et al. (2015) showed that this discrepancy is alleviated if the H I gas density in Perseus is lower than typical CNM, with $n \approx 2$–$10$ cm$^{-3}$. The analysis of Bialy et al. (2015) assumed a single H I-to-$H_2$ transition layer. Following the above discussion, a potential alternative explanation for the "too-large" H I columns in Perseus would be that there are typically two to three H I-to-$H_2$ transition layers along the Perseus sightlines.

Extragalactic observations often find an H I threshold of $\approx 10\ M_\odot$ pc$^{-2}$ (e.g., Bigiel et al. 2008; Schruba et al. 2011). This threshold was explained in the framework of a steady-state H I-to-$H_2$ transition model (K09). However, while the model applies to a single cloud, the extragalactic observations, having resolutions of the order of a kiloparsec, are not able to resolve molecular clouds, nor even large molecular complexes such as

[3] We divide their prefactor by 2. An additional factor of 1.7 comes from the normalization of the radiation fields of Habing (1968) compared to the field of Draine (1978).

W43. Interpreting the H I threshold as an H I-to-$H_2$ transition is therefore problematic. The H I threshold might be a result of two effects acting in opposite directions: (i) several H I layers along the line of sight, which increase the column density, and (ii) beam dilution by diffuse intercloud gas and WNM, which lowers the observed column densities (e.g., Shaya & Federman 1987; Paramentier 2016).

## 5. Conclusions

The main results of our paper are as follows.

1. The observed H I column densities in W43, $\Sigma_{\rm H\,I,obs} = 120$–$180\ M_\odot\ {\rm pc}^{-2}$, are very large compared to those predicted by equilibrium H I-to-$H_2$ theories, $\Sigma_{\rm H\,I} \sim 10\ M_\odot\ {\rm pc}^{-2}$ (K09; S14).
2. Realistic variations of the far-UV flux, spectral shape, volume density, or $H_2$ formation rate coefficient cannot alleviate the discrepancy between theory and observation.
3. The large observed $\Sigma_{\rm H\,I,obs}$ are naturally explained by our multislab model, in which 9–21 transition layers are superimposed along the W43 sightlines. Observations of CO, dust, and [C II] also support this model (Shibai et al. 1991).
4. Time-dependent accumulation of H I is not necessary to account for the large H I columns observed. We predict the presence of IR $H_2$ line emissions from the multiple transition layers in our picture. Such emissions would be absent for accumulating inflowing atomic gas.
5. The H I threshold often observed in extragalactic observations (e.g., Bigiel et al. 2008) may be a result of telescope beam averaging of (i) large column densities due to many H I clouds along the sightlines, with (ii) additional diffuse gas of low column density.

We thank Jouni Kainulainen, Bruce Draine, Simon Glover, Steven Federman, and Sahar Shahaf for helpful suggestions and fruitful discussions. We thank the referee for helpful comments on our manuscript. S.B. thanks the MPIA for visitor support where this research was carried out. This work was supported in part by the PBC Israel Science Foundation I-CORE Program grant 1829/12.

## Appendix

To obtain the PDF of $\alpha G$, and in particular the median $\alpha G = 17.7^{+30}_{-11.5}$ (Equation (4)), where the error corresponds to the 68.3 percentile about the median (i.e., "1-sigma"), we assume that $\log I_{\rm UV}$ and $\log(n/{\rm cm}^{-3})$ are uniformly distributed within our adopted ranges $I_{\rm UV} = 3$–$30$ and $n = 10$–$100\ {\rm cm}^{-3}$ (Section 3.1). We have chosen a uniform distribution since it is the one with maximum entropy. To obtain the PDF of $\alpha G$, let us introduce the following random variables:

$$X \equiv \log_{10}\left(\frac{I_{\rm UV}}{3}\right) \tag{8}$$

$$Y \equiv -\log_{10}\left(\frac{n}{100\ {\rm cm}^{-3}}\right) \tag{9}$$

$$Z \equiv \log_{10}\left(\frac{\alpha G}{1.8}\right). \tag{10}$$

With these definitions, $X$ and $Y$ are uniformly distributed within the range [0, 1], and $Z = X + Y$ (assuming Equation (2) with $\widetilde{\sigma}_g = 1$). The PDF of $Z$ is thus a convolution of the $X$ and $Y$ distributions, and results in the symmetric triangular distribution, with a mean of 1 and a standard deviation $1/\sqrt{6}$. This gives $\alpha G = 17.7^{+30.7}_{-11.2}$ for the median and 68.3 percentile about the median. The 95.5 and 99.7 percentiles correspond to $\alpha G = 2.9$–$108.4$ and 2.0–157.0, respectively (the ranges are symmetric about the median in log space). The PDF of $\alpha G$ may also be obtained numerically by generating large numbers of random pairs for $\{\log I_{\rm UV},\ \log(n/{\rm cm}^{-3})\}$, and then using Equation (2) to obtain the $\alpha G$ PDF. We have followed such a numerical procedure to verify the above analytic result.

## References

Anderson, L. D., Bania, T. M., Balser, D. S., et al. 2014, ApJS, 212, 1
Beuther, H., Bihr, S., Rugel, M., et al. 2016, A&A, 595, A32
Bialy, S., & Sternberg, A. 2016, ApJ, 822, 83
Bialy, S., Sternberg, A., Lee, M.-Y., Le Petit, F., & Roueff, E. 2015, ApJ, 809, 122
Bigiel, F., Leroy, A., Walter, F., et al. 2008, AJ, 136, 2846
Bihr, S., Beuther, H., Ott, J., et al. 2015, A&A, 580, A112
Black, J. H., & van Dishoeck, E. F. 1987, ApJ, 322, 412
Carlhoff, P., Luong, Q. N., Schilke, P., et al. 2013, A&A, 560, A24
Draine, B. T. 1978, ApJS, 36, 595
Draine, B. T. 2003, ApJ, 598, 1017
Draine, B. T. 2011, Physics of the Interstellar and Intergalactic Medium (Princeton, NJ: Princeton Univ. Press)
Federman, S. R., Glassgold, A. E., & Kwan, J. 1979, ApJ, 227, 466
Gillmon, K., Shull, J. M., Tumlinson, J., & Danforth, C. 2006, ApJ, 636, 891
Glover, S. C. O., & Mac Low, M.-M. 2007, ApJ, 659, 1317
Gnedin, N. Y., Tassis, K., & Kravtsov, A. V. 2009, ApJ, 697, 55
Goldsmith, P. F., Li, D., & Krčo, M. 2007, ApJ, 654, 273
Habing, H. J. 1968, BAN, 19, 421
Krumholz, M. R., McKee, C. F., & Tumlinson, J. 2008, ApJ, 689, 865
Krumholz, M. R., McKee, C. F., & Tumlinson, J. 2009, ApJ, 693, 216
Lagos, C. d. P., Crain, R. A., Schaye, J., et al. 2015, MNRAS, 452, 3815
Lee, M.-Y., Stanimirović, S., Douglas, K. A., et al. 2012, ApJ, 748, 75
Lee, M.-Y., Stanimirović, S., Murray, C. E., Heiles, C., & Miller, J. 2015, ApJ, 809, 56
Liszt, H. S. 2015, ApJ, 799, 66
McKee, C. F., & Krumholz, M. R. 2010, ApJ, 709, 308
Motte, F., Nguyen Luong, Q., Schneider, N., et al. 2014, A&A, 571, A32
Motte, F., Schilke, P., & Lis, D. C. 2003, ApJ, 582, 277
Nguyen-Luong, Q., Motte, F., Carlhoff, P., et al. 2013, ApJ, 775, 88
Ngûyen Luong, Q., Motte, F., Schuller, F., et al. 2011, A&A, 529, A41
Noterdaeme, P., Krogager, J.-K., Balashev, S., et al. 2016, A&A, in press, (arXiv:1609.01422)
Parmentier, G. 2016, ApJ, 826, 74
Reach, W. T., Dwek, E., Fixsen, D. J., et al. 1995, ApJ, 451, 188
Reach, W. T., Koo, B.-C., & Heiles, C. 1994, ApJ, 429, 672
Robertson, B. E., & Kravtsov, A. V. 2008, ApJ, 680, 1083
Savage, B. D., Bohlin, R. C., Drake, J. F., & Budich, W. 1977, ApJ, 216, 291
Schruba, A., Leroy, A. K., Walter, F., et al. 2011, AJ, 142, 37
Shaya, E. J., & Federman, S. R. 1987, ApJ, 319, 76
Shibai, H., Okuda, H., Nakagawa, T., et al. 1991, ApJ, 374, 522
Sternberg, A. 1988, ApJ, 332, 400
Sternberg, A., & Dalgarno, A. 1989, ApJ, 338, 197
Sternberg, A., Le Petit, F., Roueff, E., & Le Bourlot, J. 2014, ApJS, 790, 10S
Valdivia, V., Hennebelle, P., Gérin, M., & Lesaffre, P. 2016, A&A, 587, A76
Weingartner, J. C., & Draine, B. T. 2001, ApJ, 553, 581
Wolfire, M. G., McKee, C. F., Hollenbach, D., & Tielens, A. G. G. M. 2003, ApJ, 587, 278
Zhang, B., Moscadelli, L., Sato, M., et al. 2014, ApJ, 781, 89